photonics

MDPI

Article

Optical Properties of Black Carbon Aerosols with Different Coating Models

Yanxia Tang, Yong Huang and Keyong Zhu *

School of Aeronautic Science and Engineering, Beihang University, Beijing 100191, China; yanxiatang@buaa.edu.cn (Y.T.); huangy@buaa.edu.cn (Y.H.)
* Correspondence: zhukeyong@buaa.edu.cn

Abstract: Research on the optical properties of black carbon (BC) aerosols is highly important for investigating global climate change. A general inhomogeneous particle superposition model is developed. Inhomogeneous particles with arbitrary shapes can be constructed by this model. BC aerosols with core-shell, spherical, ellipsoid, and irregular coating models are established to explore the impact of coating shape on their optical properties. The optical properties are studied employing the discrete dipole approximation method (DDA). The influences of the morphology of BC aerosols, the coating volume fractions, and the shape of coatings on the optical properties are analyzed. The irregular coating shape causes a higher forward scattering intensity and a lower extinction cross-section. The forward scattering intensity of the core-shell model is lower than other models. The effect of the coating shape on forward scattering intensity becomes smaller as coating volume and fractal dimension increase. Consequently, assuming irregular coating as spherical coating models considered in most studies leads to inaccuracy in the optical properties of BC aerosols. It is necessary to comprehensively consider the effects of aerosol morphology and coating volume for investigating the optical properties of black carbon aerosols.

Keywords: inhomogeneous particle superposition model; black carbon aerosols; optical properties; discrete dipole approximation method

Citation: Tang, Y.; Huang, Y.; Zhu, K. Optical Properties of Black Carbon Aerosols with Different Coating Models. *Photonics* **2022**, *9*, 359. https://doi.org/10.3390/photonics9050359

Received: 27 April 2022
Accepted: 17 May 2022
Published: 19 May 2022

1. Introduction

Black carbon (BC, also known as light-absorbing carbon or soot) aerosols, generated by incomplete combustion of biomass, biofuel, and fossil fuel, are the most important component of atmospheric aerosols [1]. Black carbon aerosols have an important influence on global climate change because of their strong absorption of solar radiation [2]. After the emission of carbon dioxide, Black carbon emission is the second-largest contributor to global warming [3]. In terms of the Fifth Assessment Report of the Intergovernmental Panel on Climate Change (IPCC), significant challenges remain in accurately estimating the radiative forcing of aerosols and clouds [4]. Therefore, research on the optical properties of BC aerosols is highly important for investigating global climate change.

BC aerosol particles have fractal morphological characteristics and become heterogeneous during aging processing [5,6]. According to transmission electron microscopy (TEM) and scanning electron microscopy (SEM) figures, newly generated BC aerosol particles exist in the morphology of aggregates composed of small spheres [7]. Observations show that, during the aging process, BC aerosols always mix with other materials, for example, sulfate, water droplets, organics, dust, nitrate, and sea salt, by mutually wrapping, coating, and embedding [8,9]. Meanwhile, fresh black carbon aerosols with loose structures become compact after mixing [10–12]. Both numerical studies and experimental data have shown that coating or hygroscopic growth will greatly enhance the absorption and scattering of BC aerosols [13,14]. The enhancement may cause significant deviations in measurements of environmental black carbon concentrations [15] and brings uncertainties to the estimation of the radiation effect [11].

A lot of research has been done on inhomogeneous aggregates particles. The simplest model is to consider black carbon and non-absorptive materials as a homogenous sphere using the effective medium approximations (EMA) [16–18]. Since their optical characteristics can be easily obtained using the core-shell Mie theory, the core-shell model for a shell of weak absorption material coated on BC core is extensively employed [19]. Ackerman et al. [20] calculated the phase function and optical parameters of the concentric spherical core-shell model composed of soot core and sulfate solution shell. However, the above models ignore the fractal change of aggregates, i.e., from loose to compact structures during the aging process. For accuracy to represent the morphology, the model of the aggregate with core-shell monomers was proposed. Yin and Liu [21] combined the superposition T-matrix method with the Maxwell–Garnett (MG) formula of EMA to investigate the effects of the thickness of water coating on radiation characteristics of compact and lacy aggregates with core-shell monomers. Fan et al. [22] calculated the optical parameters of the soot aggregate composed of core-shell monomers by applying the superposition T-matrix method. The influence of water coating and morphology of aggregates was studied. More realistic and complex models are constructed in studies to calculate optical properties. The spherical or irregular coating shapes are added to fractal aggregates. Dong et al. [23] used DDA to compute the radiative characteristics of BC aerosols mixed with sulfate under four states of bare, partly coated and heavily coated soot, as well as soot with inclusion. Liu et al. [24] investigated the effects of the relative distance between centroids of BC aggregate and spherical coating as well as coating volume on their optical properties employing the multiple-sphere T-matrix method (MSTM). Kahnert et al. constructed the core grey shell (CGS) model [25] and the tunable model [26] to simulate the optical parameters and depolarization by BC aggregates with coating, respectively. For simulating different optical properties, the morphological characteristics of the two models are very different. The CGS model is a concentric core-shell sphere with high symmetry, while the tunable model is an irregular geometry with realistic morphology. Recently, Kahnert and Kanngießer [27] developed a new core-grey-shell dimer (CGS2) model to simulate optical parameters and the linear depolarization ratio simultaneously. In addition, the radiative transfer of particles in the medium has been extensively studied. The non-uniform size distribution of particles and dependent scattering affect the radiative properties of the particle-containing medium [28–30]. The DDA method considering the dependent scattering effect is applied to calculate the optical properties of BC aerosols in this paper. BC aerosols with non-uniform particle size distribution should be studied in future work.

As mentioned above, simplified black carbon aerosol models can reproduce their optical properties to some extent. However, based on SEM images, the geometries of BC aerosols are generally arbitrary and irregular [9,31], and simplified models cannot represent the sensitivity of optical properties to morphological characteristics of aerosol. Therefore, it is necessary to construct a general model for characterizing different BC aerosol states more realistically in the atmosphere. A general inhomogeneous particle superposition model is developed on the basis of the particle superposition model in this paper. Inhomogeneous particles with arbitrary shapes can be constructed by this model. BC aerosols with core-shell, spherical, ellipsoid, and irregular coating shapes are established. The optical properties are calculated by DDA. The effects of the morphology of BC aerosols, the coating volume fractions, and the shape of coatings on the optical properties are analyzed.

2. Methodology

2.1. The Modeling of Black Carbon (BC) Aerosols

Black carbon aggregates contain many small spherical primary particles (also called monomers). We construct black carbon aggregates on the basis of the particle superposition model. The advantage of the particle superposition model is that it is more convenient to describe and simulate realistic particles or aggregates with fewer modulating parameters [32]. The monomers form fractal aggregates in point-touch to explore the influence of sulfate coating in this paper.

Diffusion Limited Aggregation model (DLA) [33] is used to simulate the aggregation process. The DLA model has been extensively applied to simulate the generation of BC aggregates with fractal structure [34–36]. The advantage of this model is that it is simpler and faster than other algorithms [37]. The fractal rules are used to describe the fractal morphology of BC particles as follows [38,39]:

$$N_s = k_0 \left(\frac{R_g}{a}\right)^{D_f} \tag{1}$$

in which N_s and a are the number and radius of monomers in aggregate, respectively. The fractal prefactor k_0 and fractal dimension D_f are key parameters to characterize fractal morphology.

R_g is the radius of gyration [40], given by the following equation:

$$R_g = \frac{1}{N_S} \sum_{i=1}^{N_s} (r_i - r_0)^2 \tag{2}$$

in which r_i denotes the center position of i_{th} monomer and r_0 represents the mass center position of aggregate.

The average monomer radius of the BC aggregates is usually in the range of 0.01–0.05 μm [41]. Typical morphological parameters are chosen to simulate BC particles [24,35,42]. The k_0, N_s and a are fixed as 1.19, 100 and 15 nm in this paper. As BC ages in the atmosphere, the fractal dimensions of BC aggregates change from 1.8 in the fresh state (loose aggregates) to about 2.8 in the heavily aged state (compact aggregates) [38,43]. The morphological change of bare BC aggregates during the aging process is exhibited in Figure 1.

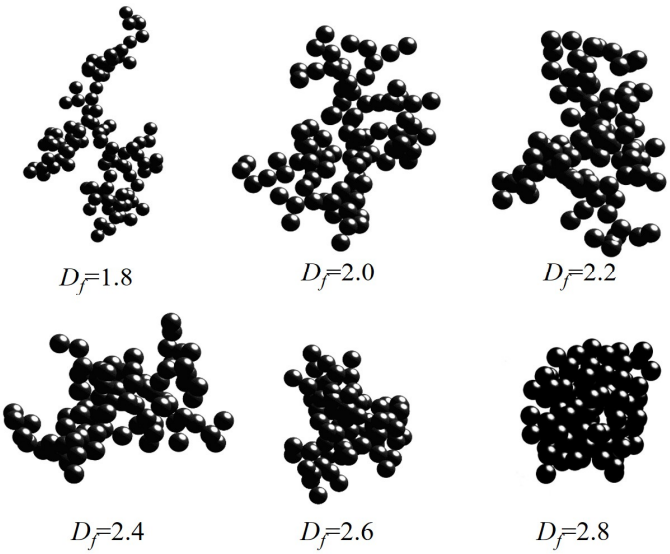

Figure 1. The morphological change of bare BC aggregates during the aging process.

The particle superposition model we proposed in the previous work can be used to simulate irregular particles with complex geometries. This model was applied to create large irregular particles [44], roughness particles [45], sintered aggregates with necking-ball structures [32], and porous particles [46]. Based on the particle superposition model, we develop the general inhomogeneous particle superposition model. This model is applied to establish BC aerosols with sulfate coatings in this paper.

The size of the sulfate coating is determined by the coating volume fraction, f_{coating} is given by:

$$f_{\text{coating}} = 1 - f_C = \frac{V_{\text{coating}}}{V_{\text{coating}} + V_{BC}} = \frac{N_{\text{coating}}}{N_{\text{coating}} + N_{BC}} \tag{3}$$

where f_{coating} is the coating volume fraction, V_{BC} denotes the volume of the BC aggregate, and V_{coating} denotes the volume of coating. Actually, the f_{coating} depends on the ratio of the number of BC dipoles N_{BC} to the sum number of BC dipoles N_{BC} and coating dipoles $N_{coating}$.

Four models of black carbon aerosols with sulfate coatings are illustrated in Figures 2 and 3. The details for constructing the models are described as follows.

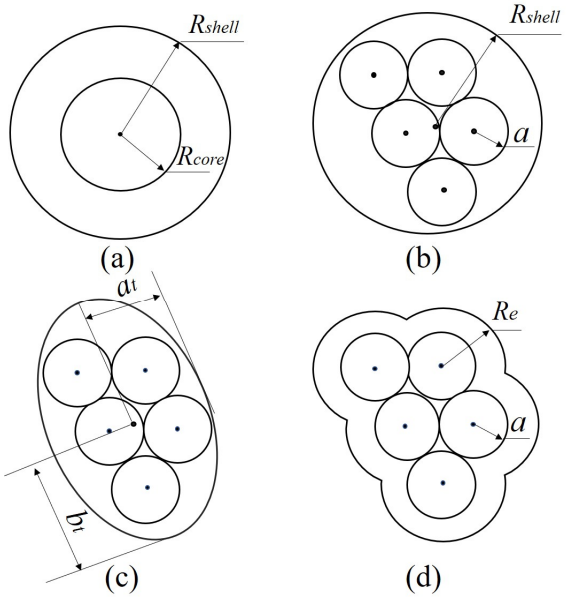

Figure 2. Illustration of models for black carbon aerosols with different sulfate coating shapes: (**a**) core-shell model, (**b**) spherical coating model, (**c**) ellipsoidal coating model, and (**d**) irregular coating model.

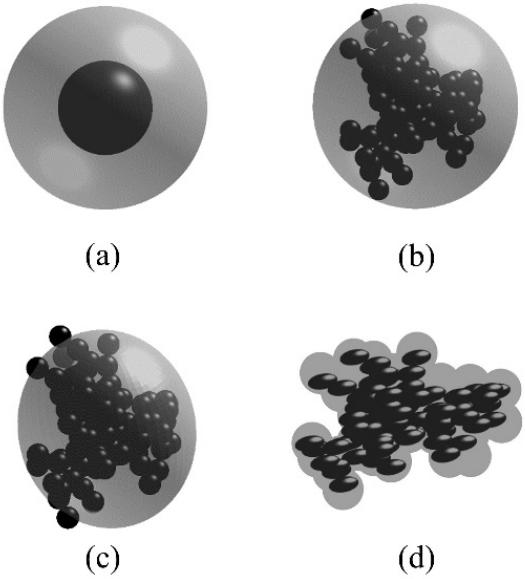

Figure 3. Models for black carbon aerosols with different sulfate coating shapes: (**a**) core-shell model, (**b**) spherical coating model, (**c**) ellipsoidal coating model, and (**d**) irregular coating model.

- the core-shell model: The BC aggregate is simplified as a homogeneous sphere core with radius $R_{\text{core}} = a(N_s)^{1/3}$, and the spherical coating is assumed to be a concentric shell with radius R_{shell}.
- the spherical coating model: First, BC aggregates with the radius of monomer a, and the monomer number N_s of are constructed according to Section 2.1. Next, we

create the spherical coating with the same center position of aggregates. The radius of spherical coating is R_{shell}. Finally, we remove the part occupied by BC aggregates in the spherical coating.

- the ellipsoidal coating model: The establishment process of this model is similar to that of the spherical coating model, except that the shape of coating is ellipsoid. The length of each axis of the ellipsoid is determined by the ratio t which is the ratio of the length of x, y and z in aggregates, i.e., $a_t : b_t : c_t = x : y : z = t$
- the irregular coating model: First, BC aggregates which are the same as the aggregates in the spherical and ellipsoidal coating model are generated. Next, we create the overlapping coating aggregates with the same monomer center as BC aggregates. The monomer radius of coating aggregates R_e is larger than the radius of BC monomer a. Finally, we remove the part occupied by BC aggregates in the overlapping coating aggregates.

The general inhomogeneous particle superposition model we proposed is flexible and versatile. The inhomogeneous particle superposition model is composed of monomer spheres. We can modulate the number and the radius of monomers, relative positions of the monomers, the center positions, and the size parameter of sulfate coating (R_{shell} in spherical coating model and core-shell model, t in ellipsoidal coating model and R_e in the irregular coating model) to simulate the target aerosols with any arbitrary coating shape and different coating volumes. In addition, the inhomogeneous particle superposition model can be applied to different coating materials by changing the material of each monomer. In this paper, we consider the effects of fractal dimension on optical properties in all models except the core-shell model during the aging process. We assume that the coating has the same center of mass as BC aggregates in the four models.

2.2. Computational Method

The discrete dipole approximation (DDA), an electromagnetic volume integral-based method, is a popular method for computing radiation characteristics of particles with arbitrary geometries and inhomogeneous material [47,48]. DDA was applied for calculating the optical properties using DDSCAT 7.3.0 [49–53] jointly developed by Draine and Flatau from America in this paper.

The parameters that need to be set in DDSCAT include the shape of the particles, the number of dipoles, the complex refractive index, and the radius of a given spherical particle or the volume-equivalent radius R_{eff} of a non-spherical particle.

A target with volume V is described by an array of N dipoles. The volume-equivalent radius R_{eff} is defined as follows [49]:

$$R_{eff} = \left(\frac{3N}{4\pi}\right)^{1/3} d \tag{4}$$

where d denotes the spacing of a cubic lattice.

Considering the practical CPU speed and computer memory, the number of dipoles is limited to $N < 10^6$ [50]. In order to calculate the cross-section and scattering phase function accurately, $|m|kd < 0.5$ is needed:

$$R_{eff} < 4.94 \frac{\lambda}{|m|} \left(\frac{N}{10^6}\right)^{1/3} \tag{5}$$

in which m denotes the complex refractive index and $k = 2\pi/\lambda$ denotes the wavenumber. For this reason, this paper ensures $|m|kd < 0.1$ for each model.

The extinction efficiency factor Q_{ext}, absorption efficiency factor Q_{abs}, and scattering efficiency factor Q_{sca} can be computed by DDSCAT 7.3.0, and the corresponding extinction

cross-section C_{ext}, absorption cross-section C_{abs}, and scattering cross-section C_{sca} [54] can be obtained by the following equation:

$$C_{ext} = Q_{ext}\pi R_{eff}^2 \tag{6}$$

$$C_{abs} = Q_{abs}\pi R_{eff}^2 \tag{7}$$

$$C_{sca} = Q_{sca}\pi R_{eff}^2 \tag{8}$$

ω denotes the single-scattering albedo is defined as follows [55]:

$$\omega = \frac{C_{sca}}{C_{ext}} \tag{9}$$

The asymmetry parameter g [56,57] depicts the directionality of the scattered energy distribution. It is defined by

$$g = <\cos\theta> = \frac{1}{4\pi}\int_{4\pi}\Phi(\theta)\cos\theta d\Omega \tag{10}$$

The Mueller matrix $\boldsymbol{P}$ describes the scattering characteristics of the targets, which is related to the Stokes vectors of the incident and scattered radiation. It is defined as:

$$I_{sca} = \frac{C_{sca}}{4\pi d^2}\boldsymbol{P}\cdot I_0 \tag{11}$$

The conversion between a scattering matrix $\boldsymbol{S}$ given by DDA and a phase matrix [58] is required:

$$\boldsymbol{P} = \frac{4\pi}{k^2 C_{sca}}\boldsymbol{S} \tag{12}$$

We focus on the Mueller matrix elements P_{11}, $-P_{12}/P_{11,}$ and P_{22}/P_{11}. P_{11} means normalized phase function, representing the scattering intensity distribution. The Mueller matrix element ratio $-P_{12}/P_{11}$ denotes the linear polarization degree of scattering light when the incident light is unpolarized light. The P_{22}/P_{11}, a depolarization-related term, represents the non-spherical degree of geometry, and the P_{22}/P_{11} of a sphere is equal to 1.

3. Results and Discussion

The incident wavelength is set as 550 nm. At this wavelength, the refractive index of BC is $m = 1.73 + 0.59i$ [24,59]. The refractive index of sulfate coating is chosen as $1.43 + 0i$ [23,24]. For each BC aerosol model under different circumstances shown in Figure 3, five stochastic realizations of geometry are generated. We average the computational results over the five realizations to reflect their general optical properties.

3.1. Sensitivity Studies of the Numbers of Target Orientations

For evaluating the angular integration more accurately and applying Simpson's rule, odd numbers of orientation angles should be selected. Considering the computational cost and precision, the optimum numbers of discrete orientations of Euler angles β, Θ and Φ have to be chosen. Sensitivity studies are implemented with the optical properties of BC aggregates with $D_f = 2.2$ and BC aerosols with spherical sulfate coating. The coating volume fraction is assumed as 0.8.

Figure 4, Tables 1 and 2 show the influence on extinction cross-section C_{ext}, single-scattering albedo ω, and asymmetry parameter g of BC aggregates with different discrete orientation numbers. As shown in Figure 4, C_{ext}, ω, and g of aggregate and BC aerosols with spherical coating are almost constant when the orientation number is greater than 343 ($7 \times 7 \times 7$). Observing the calculation results in Tables 1 and 2, the relative error δ of C_{ext}, ω, and g is close to 0 as the number of directions is greater than 729 ($9 \times 9 \times 9$). It

is found that averaging over 729 ($N_\beta \times N_\Theta \times N_\Phi = 9 \times 9 \times 9$) discrete orientations results in enough accuracy for optical properties.

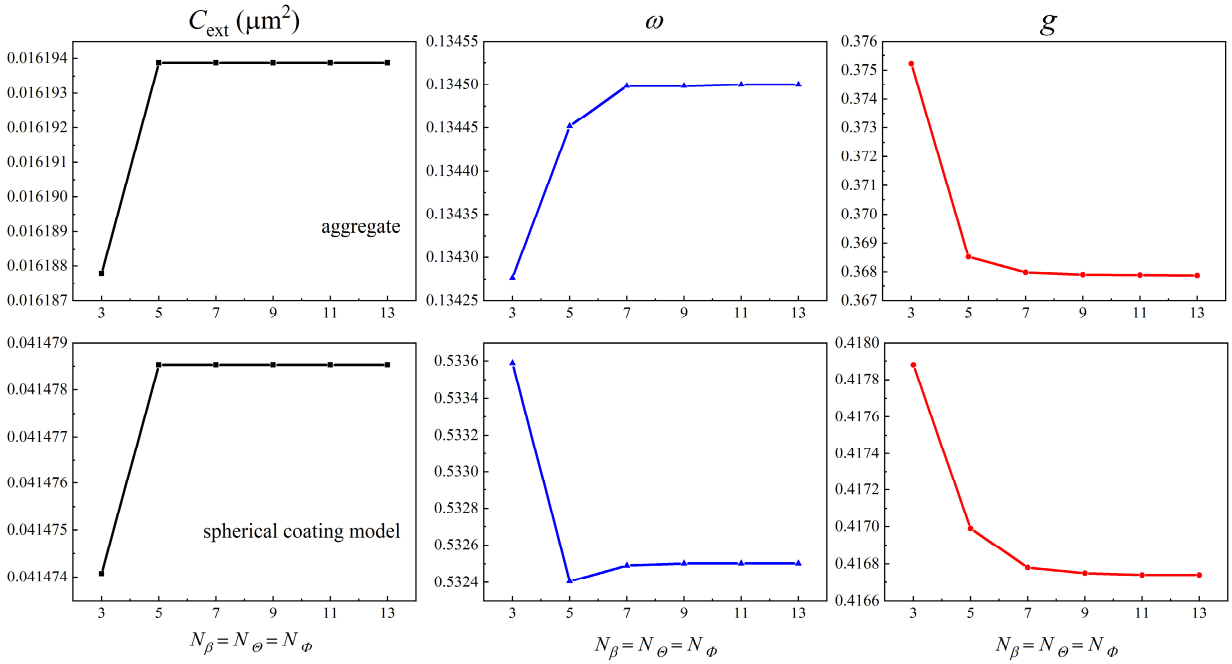

Figure 4. Extinction cross section C_{ext}, single-scattering albedo ω, and asymmetry parameter g of BC aggregates and BC aerosols with spherical coating for different numbers of orientations.

Table 1. Extinction cross-section C_{ext}, single-scattering albedo ω, and asymmetry parameter g of BC aggregates with different discrete orientation numbers.

Numbers $N_\beta \times N_\Theta \times N_\Phi$	$C_{ext} \times 10^{-2}$ μm^2	$\delta_{C_{ext}}$ %	ω	δ_ω %	g	δ_g %
3 × 3 × 3	1.61878	-	0.13428	-	0.37522	-
5 × 5 × 5	1.61939	0.0376	0.13445	0.13038	0.36852	−1.7856
7 × 7 × 7	1.61939	0	0.13450	0.03495	0.36799	−0.1438
9 × 9 × 9	1.61939	0	0.13450	0	0.36790	−0.0245
11 × 11 × 11	1.61939	0	0.13451	0.00699	0.36790	0
13 × 13 × 13	1.61939	0	0.13451	0	0.36790	0

Table 2. Extinction cross-section C_{ext}, single-scattering albedo ω, and asymmetry parameter g of BC aerosols with spherical coating for different discrete orientation numbers.

Numbers $N_\beta \times N_\Theta \times N_\Phi$	$C_{ext} \times 10^{-2}$ μm^2	$\delta_{C_{ext}}$ %	ω	δ_ω %	g	δ_g %
3 × 3 × 3	4.14741	-	0.53359	-	0.41788	-
5 × 5 × 5	4.14785	0.01074	0.53241	−0.22200	0.41699	−0.21298
7 × 7 × 7	4.14785	0	0.53249	0.01613	0.41678	−0.05036
9 × 9 × 9	4.14785	0	0.53250	0.00202	0.41675	−0.00960
11 × 11 × 11	4.14785	0	0.53250	0	0.41674	0
13 × 13 × 13	4.14785	0	0.53250	0	0.41674	0

As can be seen from the calculation results in Figure 5, the numbers of discrete orientations have little influence on the phase function P_{11} for BC aggregates and BC aerosols with spherical coating. The forward scattering overlaps under different numbers of discrete orientations. The backscattering almost coincides when the number of directions is greater than 5 × 5 × 5. The depolarization-related term P_{22}/P_{11} also almost coincides

when the number of directions is greater than 5 × 5 × 5, as shown in the rightmost panel in Figure 5. The degree of linear polarization $-P_{12}/P_{11}$ coincides under different numbers of orientations, which shows that the $-P_{12}/P_{11}$ is less sensitive to orientation numbers. Overall, the optical properties of BC aerosols were calculated by averaging over 729 (9 × 9 × 9) discrete orientations for accuracy.

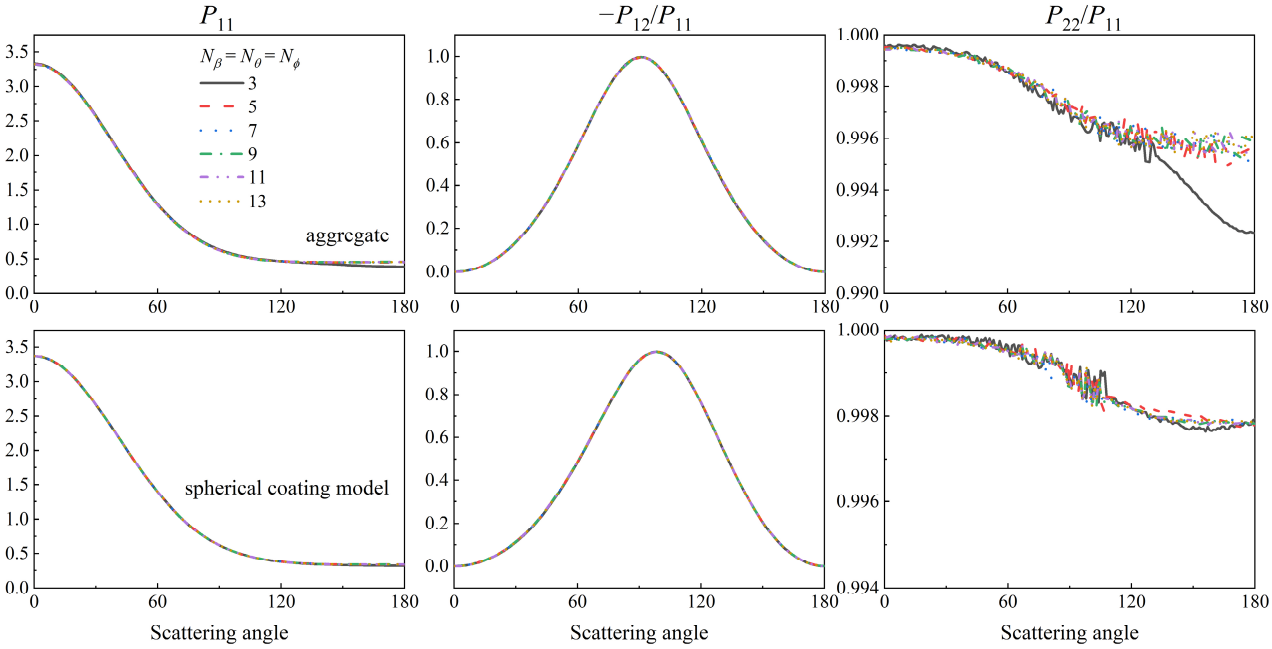

Figure 5. Mueller matrix elements of BC aggregates and BC aerosols with spherical coating for different discrete orientation numbers.

3.2. Spherical Coating Model for BC Aerosols with Different Coating Volumes

For obtaining the influence of coating volumes on the optical properties of BC aerosols, BC aerosols are assumed as spherical coating models, as shown in Figures 2b and 3b. The volume fractions of coating are 0, 0.3, 0.5, 0.7,0.8, 0.9 and 0.95. In addition, we also consider the morphology of BC aggregates during the aging process. The fractal dimensions D_f of aggregates are set as 1.8, 2.0, 2.2, 2.4, 2.6, 2.8. With different sulfate coating volumes, the effects of BC aggregates partially or fully embedded in the coating on optical properties are studied.

Figure 6 depicts the C_{ext}, C_{abs}, ω and g of BC aerosols as a function of coating volume fraction. The optical properties with different D_f have the same trends as f_{coating} increases. The C_{ext}, C_{abs} and ω increase with the increase of the coating volume. The asymmetry factor g does not increase monotonically with the increase of coating volume. The g decreases first and then increases as the coating volume increases, which is mainly determined by the mixing state of BC aggregates and coating. With the coating volume fraction reaching 0.95, g increases to about 0.65 due to the increase in coating volume, suggesting that the forward scattering becomes more dominant. Although the volume of black carbon is fixed, the absorption cross-section of the BC aerosol increases obviously because of the "lensing effects" [36]. The increased single scattering albedo reflects that BC aerosols show a stronger scattering enhancement than absorption. The larger coating volume induces stronger scattering, so the single-scattering albedo ω increases from less than 0.2 to about 0.85 which indicates that the absorption dominant particles gradually become the scattering dominant particles. The aging of BC also affects the optical properties of BC aerosols. Compact aggregates induce a larger extinction and absorption cross-section than loose aggregates at the same coating volume fraction. It is because the larger D_f causes stronger electromagnetic interaction led by the superposition of the scattered field among the monomers and the probability of absorption increases with the shrinkage of

an aggregated particle [22]. When the coating volume fraction is greater than 0.9, the extinction cross-sections with different D_f coincide. When the volume fraction is less than 0.8, the larger D_f leads to greater single scattering albedo. With the volume fraction greater than 0.8, smaller D_f shows greater ω. In addition, asymmetry factor g decreases with the increase of D_f. The analysis shows that both coating and BC aggregate have an impact on the optical properties of BC aerosol. Therefore, to investigate the optical properties of BC aerosols, the effects of coating and BC aggregate should be considered together.

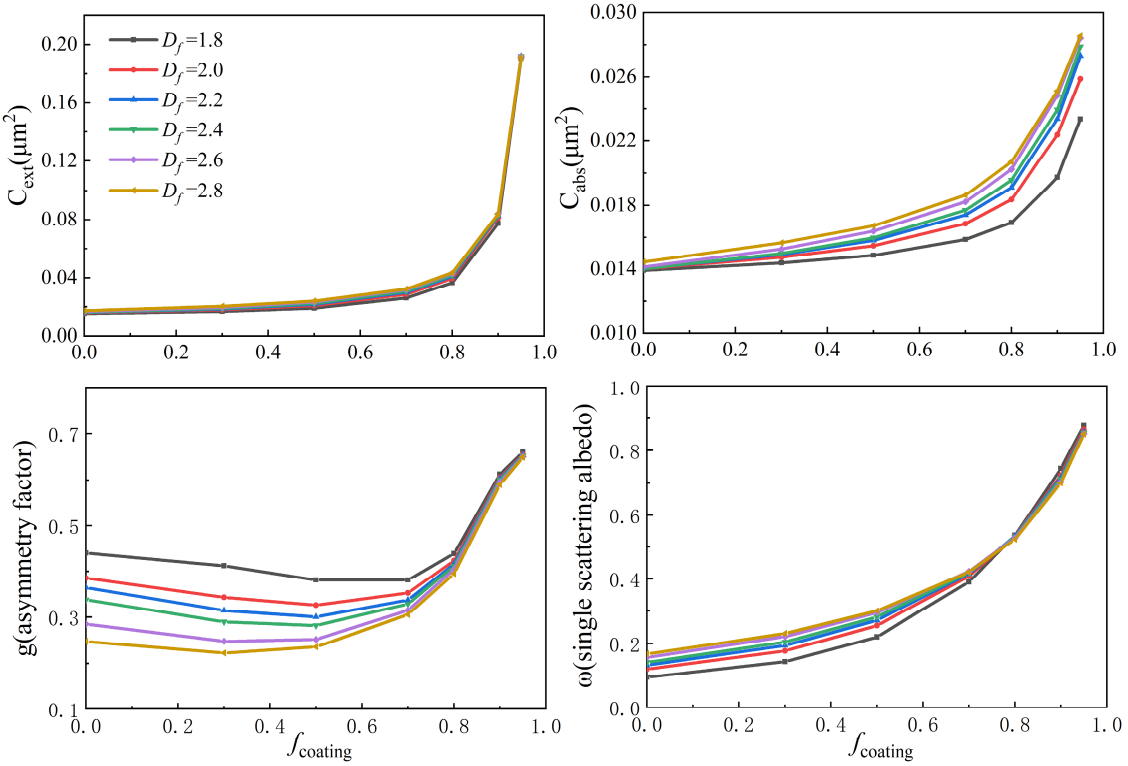

Figure 6. Optical properties of BC aerosols with spherical coating with different coating volume fractions.

The effects of coating volume fractions on the phase function P_{11} of BC aerosols with different fractal dimensions are depicted in Figure 7. The phase function P_{11} with different fractal dimensions shows a similar angular variation trend. The forward scattering intensity is stronger than the backscattering intensity. The angular patterns of P_{11} with a small coating volume fraction are smoother. P_{11} is sensitive to the coating volume. Scattering intensity does not increase monotonically as the coating volume fraction increases. Figure 8 shows the variation of the forward scattering intensity (at scattering angle = 0°) as the coating volume fraction increases. The forward scattering intensity first decreases and then increases with the increase of coating volume. This is because the BC aggregate and coating work together to affect the phase function. The P_{11} of BC aerosols can be understood as the average of BC core and coating, as analyzed in [24]. The forward scattering peak of BC aerosols at a small $f_{coating}$ is weaker than that of the bare BC aggregates. The forward scattering peak of BC aerosol increases as the coating volume increases, when the coating is dominant. The smaller the D_f, the stronger the forward scattering intensity of BC aerosol is at the same coating volume fraction.

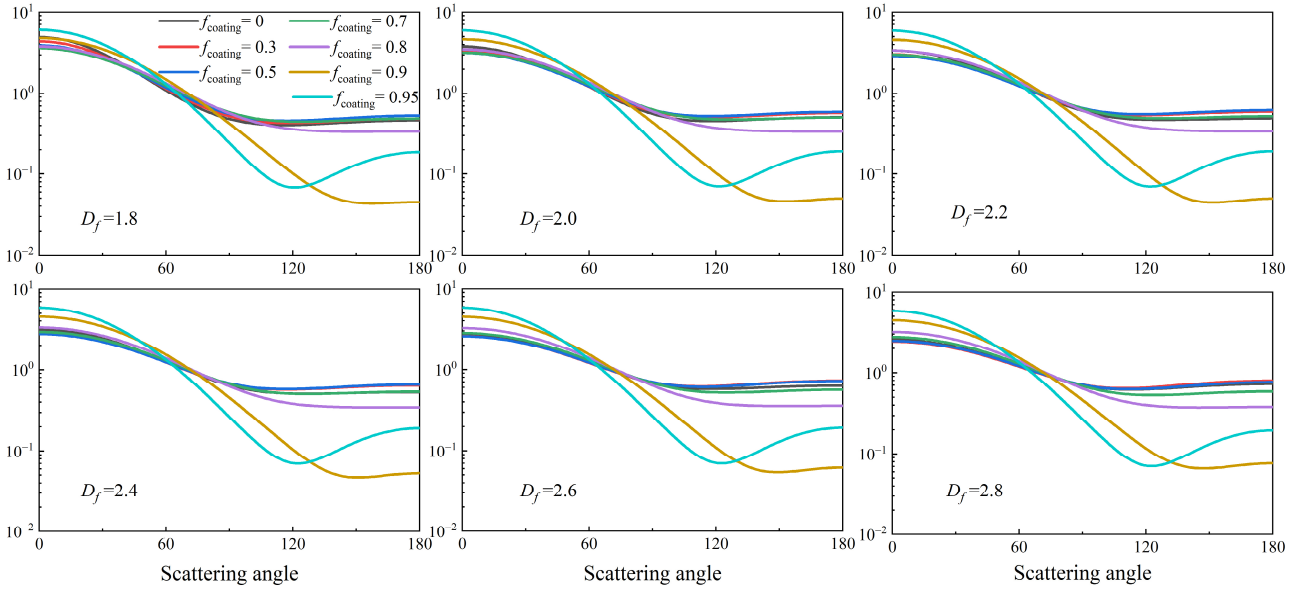

Figure 7. Scattering phase function P_{11} of BC aerosols with different coating volume fractions.

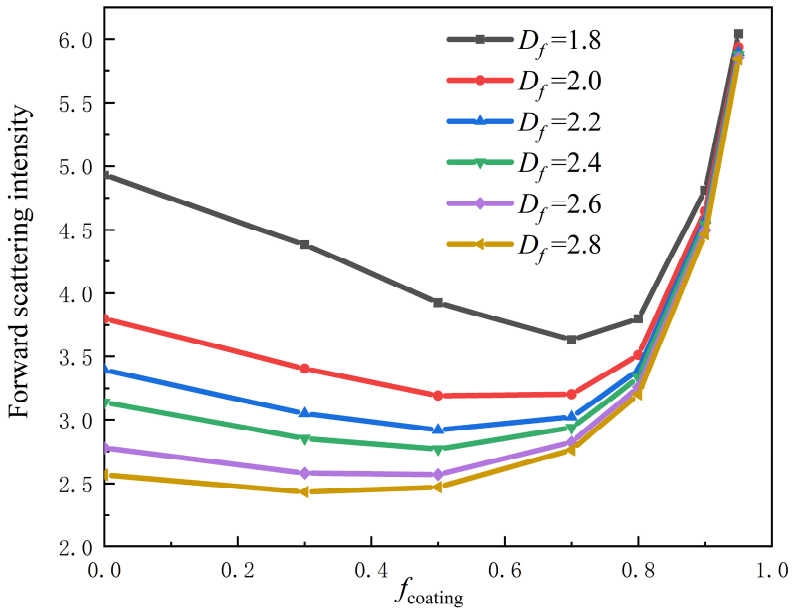

Figure 8. Forward scattering intensity (P_{11} at scattering angle = 0°) of BC aerosols with different coating volume fractions.

Figure 9 illustrates the linear polarization degree $-P_{12}/P_{11}$ of BC aerosols with different coating volume fractions. When $f_{\text{coating}} \leq 0.9$, due to the small size parameter χ ($\chi = 2\pi R_{eff}/\lambda$), the degree of linear polarization $-P_{12}/P_{11}$ shows a Rayleigh bell shape and it also can be seen that the "peak moving backward" phenomenon, that is the location of maximal linear polarization moves to larger scattering angles with an increase of coating. The Rayleigh characteristics disappear and peaks and valleys show in the linear polarization degree when $f_{\text{coating}} > 0.9$. The $-P_{12}/P_{11}$ of BC aerosols with different coating volume fractions are similar in different D_f, which indicates that D_f is not sensitive to $-P_{12}/P_{11}$ of BC aerosols.

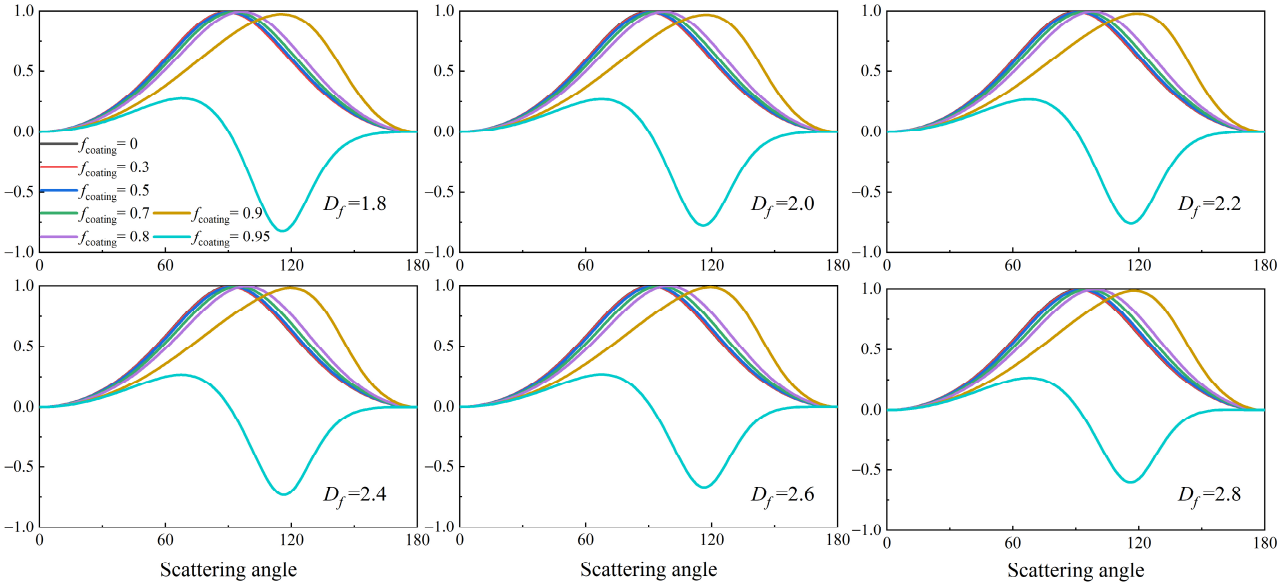

Figure 9. Mueller matrix element $-P_{12}/P_{11}$ of BC aerosols with different coating volume fractions.

Figure 10 shows the angular patterns of the depolarization-related term P_{22}/P_{11} with different coating volume fractions. With increasing the coating fraction, the mixing state of the BC aggregate and coating gradually approaches the spherical shape, which results in the P_{22}/P_{11} gradually approaching 1. The P_{22}/P_{11} represents the sphericity of geometry, and the P_{22}/P_{11} of a sphere is equal to 1. Moreover, fractal dimensions D_f also have an effect on P_{22}/P_{11}. Larger D_f causes the P_{22}/P_{11} close to 1. Thus, the mixing state of BC aggregate and coating has an influence on the Mueller matrix elements of BC aerosols.

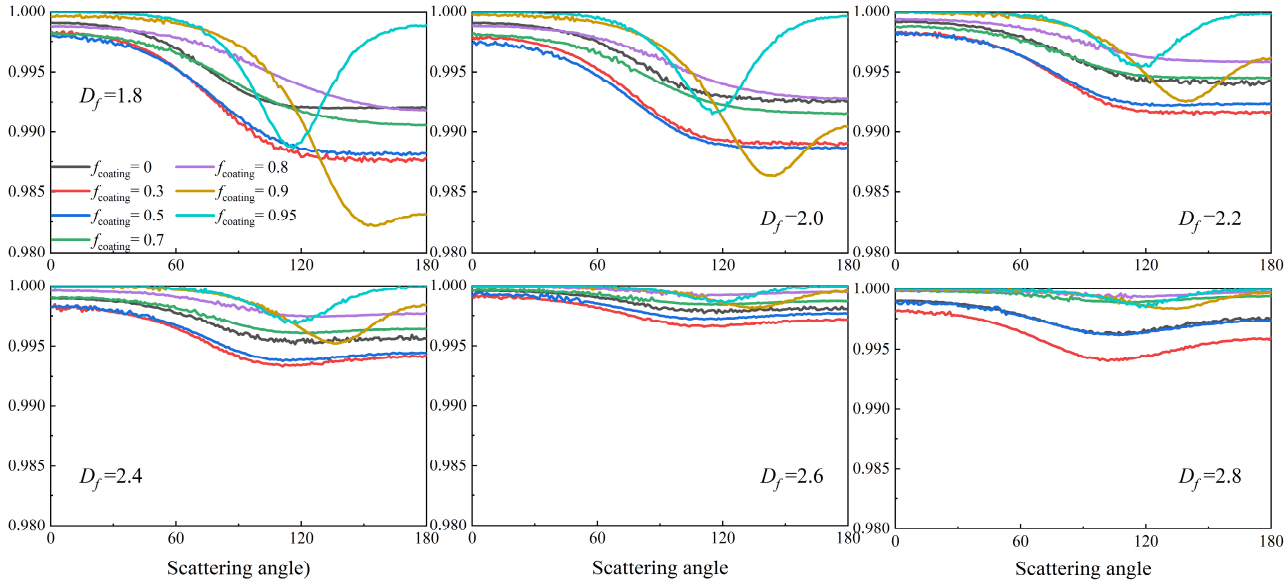

Figure 10. Mueller matrix element P_{22}/P_{11} of BC aerosols with different coating volume fractions.

3.3. BC Aerosols with Different Coating Models

The coating volume has a great influence on the optical properties of BC aerosols as illustrated in the previous section. Only the spherical coating model has been considered. Nevertheless, transmission or scanning microscopic images show that the geometry of BC aerosol is irregular during the aging process. In order to further discuss the impact of the coating shape on optical properties, we establish four models as shown in Figure 3,

and analyze their optical properties. In addition, we also consider the morphology of BC aggregates so that the D_f is set as 1.8, 2.2, and 2.8. The f_{coating} are 0.5, 0.7 and 0.9.

Figure 11 describes the influences of sulfate coating shapes on the optical properties. It can be concluded that the coating shape affects the optical properties of BC aerosols. The extinction cross-section C_{ext} and single-scattering albedo ω increase as the coating volume increases, whereas the asymmetry parameter g does not increase monotonically. This is consistent with the result of Section 3.2. The optical properties of the spherical coating model are almost the same as those of the ellipsoidal coating model. So, the spherical coating model and the ellipsoidal coating model can replace each other, when studying the optical properties of BC aerosols. The larger D_f, the closer the optical properties of the spherical and the ellipsoidal coating model are to the core-shell model. It is because that large D_f causes compact aggregate whose shape is close to the sphere. The C_{ext} of the core-shell model is the largest among all shapes. The results indicate that ignoring the fractal structure of the BC core and assuming aggregates as spheres overestimate extinction cross-sections. The C_{ext} of the irregular coating model is the smallest. This result shows that the irregular shape of the coating leads to a lower extinction cross-section. The single-scattering albedos of the spherical and the ellipsoidal coating model are larger than the irregular coating model and lower than the core-shell mode at a small coating volume fraction ($f_{\text{coating}} = 0.5$). However, when f_{coating} is greater than 0.7, the result is the opposite. The asymmetry parameters of BC aerosols are greater than 0, suggesting that scattering of the forward scattering is dominant. The g of the irregular coating model is the largest at $f_{\text{coating}} = 0.3$, and the smallest at $f_{\text{coating}} = 0.9$. In conclusion, assuming irregular coating as spherical coating models considered in most studies leads to the inaccuracy in the optical properties of BC aerosols. It is necessary to comprehensively consider the influences of coating volume and aerosol morphology for studying the optical properties of BC aerosols.

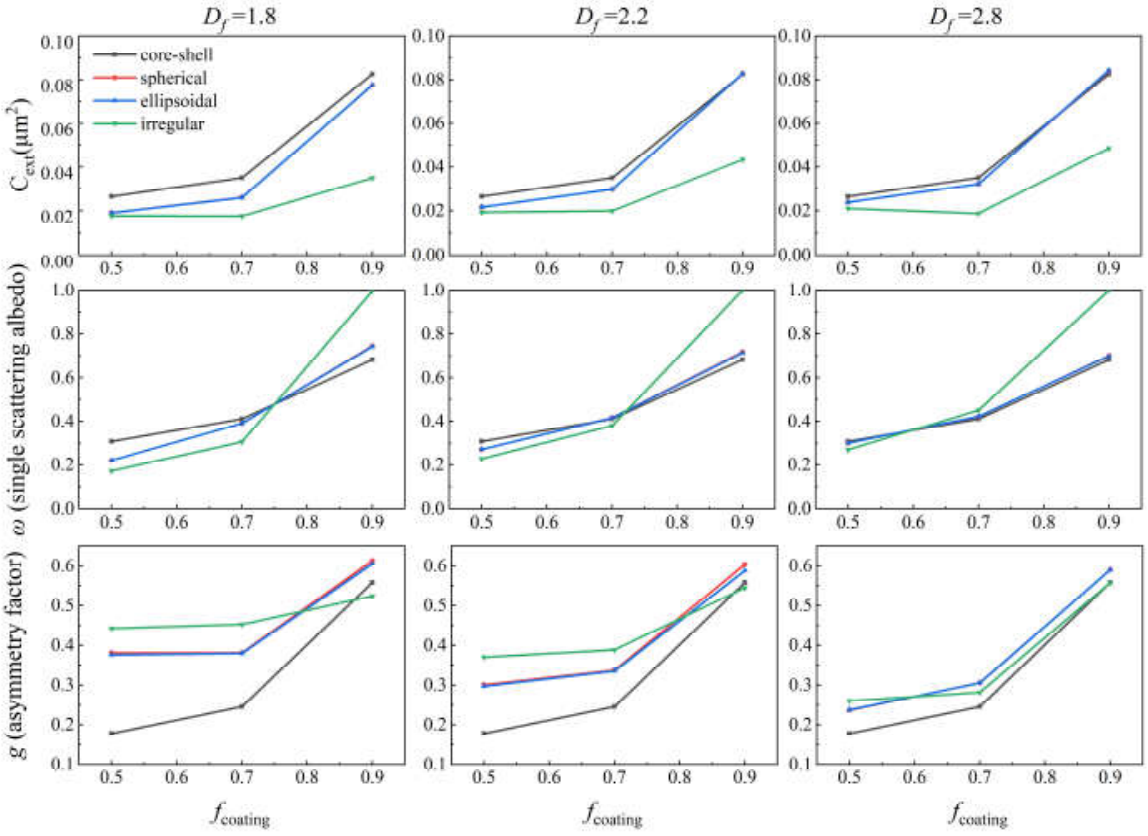

Figure 11. Optical properties of BC aerosols with different coating models.

Figure 12 depicts the scattering phase function P_{11} with different coating models. It can be seen from the figures that as the $f_{coating}$ increases, the gap between the forward and the backward scattering becomes larger. The forward scattering intensity of the core-shell model is lower than other models. Therefore, neglecting the fractal structure of BC aerosols can result in underestimating forward scattering. The scattering phase function P_{11} of spherical and ellipsoidal models almost coincide, indicating that they have the same influence on the scattering phase function. The forward scattering intensity of the irregular coating model is higher than other models. Its most irregular shape may be responsible for this. The rise of coating volume fractions leads to a decrease in the difference in forwarding scattering intensity among different shapes. Besides, at the same coating volume fractions, larger D_f also leads to a decrease in the difference in forward scattering intensity among different shapes. In summary, the coating shapes affect the phase function of the BC aerosols and the influence of the coating shape on forward scattering intensity becomes smaller as coating volume fractions and D_f increase.

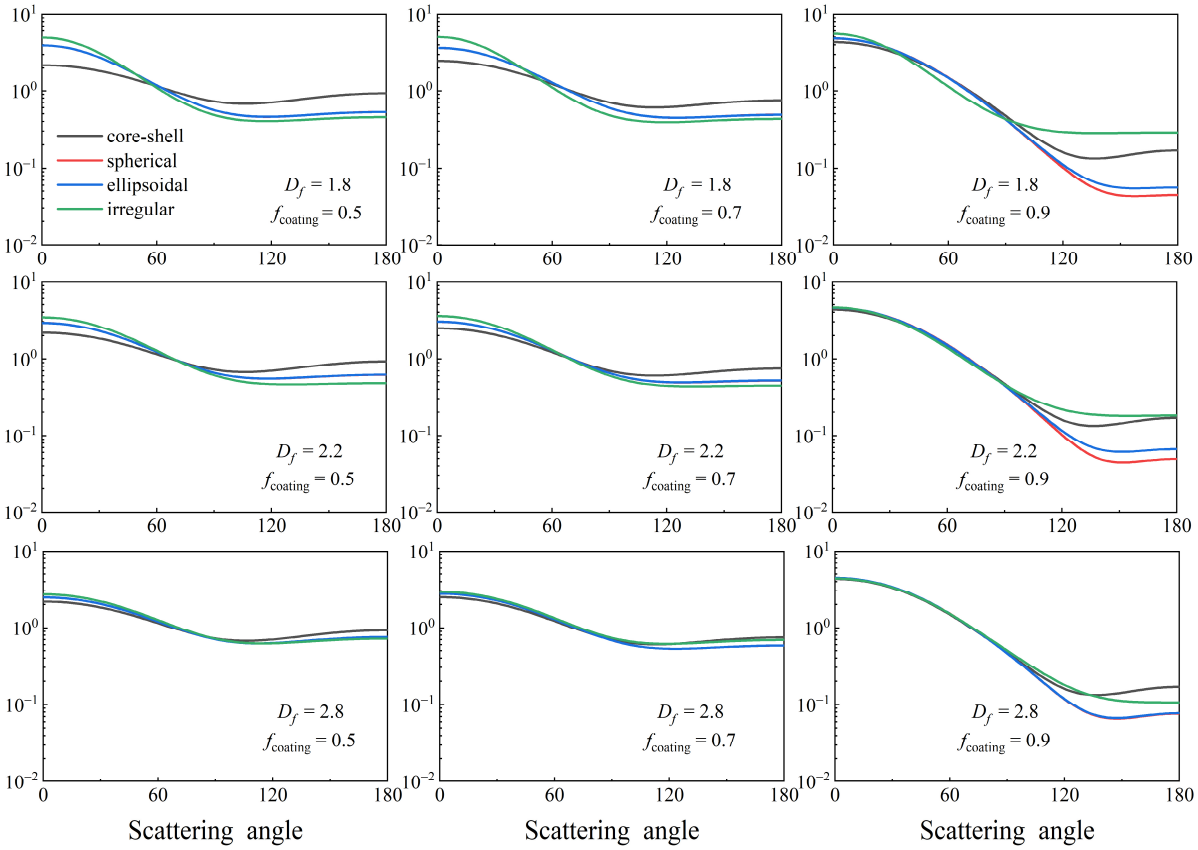

Figure 12. Phase function P_{11} of BC aerosols with different coating models.

Figure 13 illustrates the differences in linear polarization $-P_{12}/P_{11}$ among different coating models. In all models, linear polarization is basically Rayleigh bell-like with the maximum close to 1, and as the coating volume fractions $f_{coating}$ increases, the location of maximal shifts from $\theta = 90°$ to larger scattering angles. This result is consistent with the result shown in Section 3.2 for "peak moving backward" phenomenon. The peak of the irregular coating model is at a smaller scattering angle than other shapes under the same coating volume. In addition, the $-P_{12}/P_{11}$ of BC aerosols with different coating volume fractions are similar under different D_f.

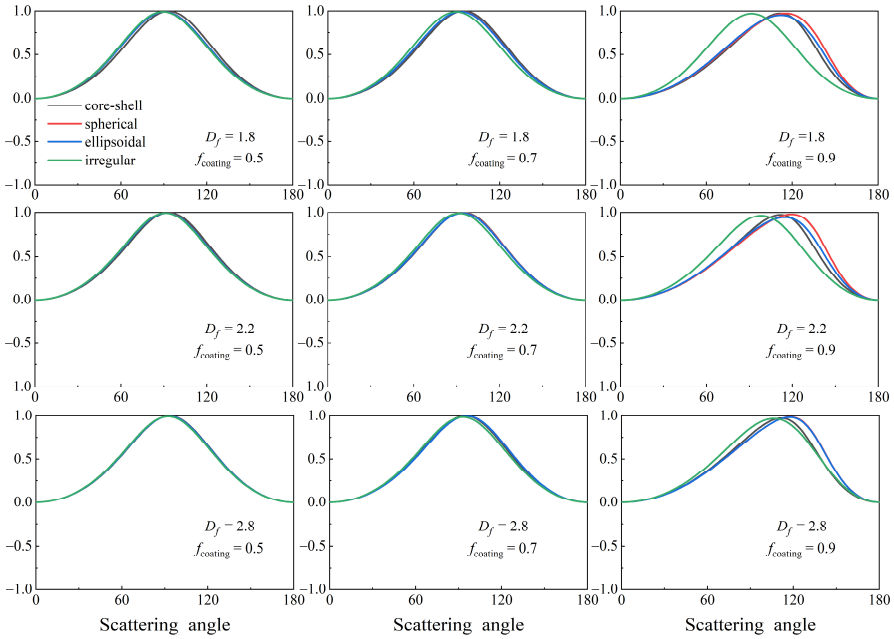

Figure 13. Linear polarization $-P_{12}/P_{11}$ of BC aerosols with different coating models.

Figure 14 describes the P_{22}/P_{11} of BC aerosols with different coating models. Since the morphology of BC aerosols with the core-shell model is spherical, the P_{22}/P_{11} of the core-shell model is almost equal to 1. The elements P_{22}/P_{11} of compact aggregates are closer to 1 than loose aggregates at the same coating volume fraction. The elements P_{22}/P_{11} of BC aerosols with spherical coating model, ellipsoidal coating model, and irregular coating model are close to each other at $f_{\text{coating}} = 0.5$. When f_{coating} is greater than 0.5, the P_{22}/P_{11} is different in different coating models. The P_{22}/P_{11} of the spherical coating model is the largest, followed by the ellipsoidal coating model and the P_{22}/P_{11} of the irregular coating model is the smallest, except for the core-shell model. In conclusion, the more irregular the morphology of BC aerosol leads to the smaller the P_{22}/P_{11}.

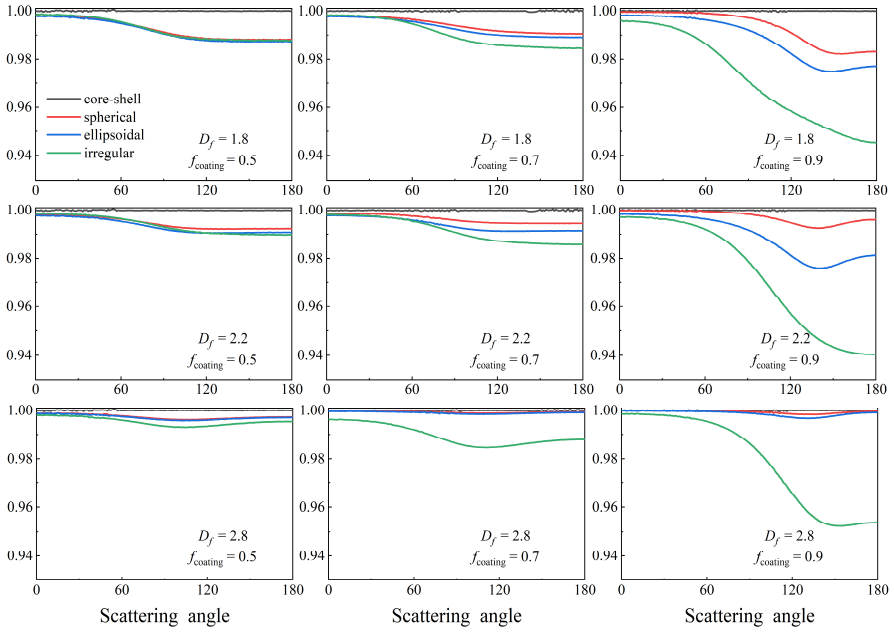

Figure 14. Mueller matrix elements P_{22}/P_{11} of BC aerosols with different coating models.

4. Conclusions

BC aerosols with core-shell, spherical, ellipsoid, and irregular coating models are established by the general inhomogeneous particle superposition model we developed in this paper. The shape of the BC core, that is, different fractal dimensions or assuming a spherical shape, the sulfate coating shape, and the coating volume fractions affect the optical properties of BC aerosols.

The influences of coating volumes on the optical properties of BC aerosols are investigated by assuming that BC aerosols are spherical coating models. The C_{ext}, C_{abs}, and ω increase as the coating volume increases. The g decreases first and then increases as the coating volume increases. The forward scattering intensity first decreases and then increases with increasing the coating volume fraction. The angular patterns of P_{11} with a small coating volume fraction are smoother. When $f_{\text{coating}} \leq 0.9$, the degree of linear polarization $-P_{12}/P_{11}$ shows a Rayleigh bell shape and the "peak moving backward" phenomenon also can be seen with the increase of coating volume. The features disappear and peaks and valleys appear in the linear polarization degree when $f_{\text{coating}} > 0.9$. With the increase of coating volume fraction, the mixing state of the BC aggregate and coating gradually approaches the spherical shape, which results in the P_{22}/P_{11} gradually approaching 1.

The coating shape influences the optical properties of BC aerosols. The optical properties of the spherical coating model are very close to those of the ellipsoidal coating model. So, the spherical and the ellipsoidal coating model can replace each other when studying the optical properties of BC aerosols. Ignoring the fractal structure of BC aggregate and assuming aggregates as spheres overestimate extinction cross-sections. The irregular shape of the coating leads to a lower C_{ext}. The single-scattering albedos of the spherical and ellipsoidal coating model are larger than the irregular coating model and lower than the core-shell mode at a small coating volume fraction ($f_{\text{coating}} = 0.5$). However, when f_{coating} is greater than 0.7, the result is the opposite. The g of the irregular coating model is the largest at $f_{\text{coating}} = 0.3$, and the smallest at $f_{\text{coating}} = 0.9$. Among all the models, the forward scattering intensity of the core-shell model is the lowest and the irregular coating model is the highest. The influence of the coating shape on forward scattering intensity becomes smaller as coating volume fractions and D_f increase. The peak of $-P_{12}/P_{11}$ of the irregular coating model is at a smaller scattering angle than other shapes under the same coating volume. The more irregular the morphology of BC aerosol leads to the smaller the P_{22}/P_{11}.

Besides, D_f also affects the optical properties. The compact aggregates induce a larger extinction and absorption cross-section than loose aggregates at the same coating volume fraction. Asymmetry factor g and the forward scattering intensity of BC aerosol decrease with the increase of D_f. The larger D_f causes the P_{22}/P_{11} close to 1 and the closer the optical properties of the spherical and the ellipsoidal coating model are to the core-shell model.

Consequently, assuming irregular coating as spherical coating models considered in most studies leads to inaccuracy in the optical properties of BC aerosols. It is necessary to comprehensively consider the influences of aerosol morphology and coating volume for studying the optical properties of BC aerosols. Establishing different BC aerosols models based on different morphologies in nature can more accurately calculate the optical properties. The general inhomogeneous particle superposition model we developed provides a general method to construct different geometries and materials of inhomogeneous particles. In this paper, we assume the coating and the BC aggregate have the same center of mass, whereas the relative position of their center of mass also affects the optical properties of BC aerosols [23,24]. The effects of the relative distance between aggregate and coating on the optical properties of BC aerosols can be further verified in future research.

Author Contributions: Conceptualization, Y.H. and K.Z.; methodology, Y.T.; software and validation, Y.T.; writing-original draft preparation, Y.T.; supervision and project administration, Y.H. and K.Z.; funding acquisition, Y.H. and K.Z. All authors have read and agreed to the published version of the manuscript.

Funding: This work was supported by the National Natural Science Foundation of China (Grant Nos. 51876004 and 52176051) and Fundamental Research Funds for Central Universities (Grant No. YWF-21-BJ-J-818).

Institutional Review Board Statement: Not applicable.

Informed Consent Statement: Not applicable.

Data Availability Statement: Not applicable.

Acknowledgments: Bruce T. Draine and Piotr J. Flatau are acknowledged for making their DDA code publicly available: http://ddscat.wikidot.com/downloads (accessed on 25 March 2015).

Conflicts of Interest: The authors declare no conflict of interest.

References

1. Bond, T.C.; Sun, H. Can Reducing Black Carbon Emissions Counteract Global Warming? *Environ. Sci. Technol.* **2005**, *39*, 5921–5926. [CrossRef] [PubMed]
2. Liu, F.; Wong, C.; Snelling, D.R.; Smallwood, G.J. Investigation of Absorption and Scattering Properties of Soot Aggregates of Different Fractal Dimension at 532 nm Using RDG and GMM. *Aerosol Sci. Technol.* **2013**, *47*, 1393–1405. [CrossRef]
3. Ramanathan, V.; Carmichael, G. Global and regional climate changes due to black carbon. *Nat. Geosci.* **2008**, *1*, 221–227. [CrossRef]
4. IPCC 2013; Stocker, T.; Qin, D.; Plattner, G.-K.; Tignor, M.; Allen, S.K.; Boschung, J.; Nauels, A.; Xia, Y.; Bex, V.; et al. *Climate Change 2013. The Physical Science Basis. Contribution of Working Group I to the Fifth Assessment Report of the Intergovernmental Panel on Climate Change*; Cambridge University Press: Cambridge, UK; New York, NY, USA, 2013; 1535p. [CrossRef]
5. Jacobson, M.Z. Strong radiative heating due to the mixing state of black carbon in atmospheric aerosols. *Nature* **2001**, *409*, 695–697. [CrossRef]
6. Shiraiwa, M.; Kondo, Y.; Iwamoto, T.; Kita, K. Amplification of Light Absorption of Black Carbon by Organic Coating. *Aerosol Sci. Technol.* **2010**, *44*, 46–54. [CrossRef]
7. Wentzel, M.; Gorzawski, H.; Naumann, K.H.; Saathoff, H.; Weinbruch, S. Transmission electron microscopical and aerosol dynamical characterization of soot aerosols. *J. Aerosol Sci.* **2003**, *34*, 1347–1370. [CrossRef]
8. Li, J.; Pósfai, M.; Hobbs, P.V.; Buseck, P.R. Individual aerosol particles from biomass burning in southern Africa: 2, Compositions and aging of inorganic particles. *J. Geophys. Res. Atmos.* **2003**, *108*, 8484. [CrossRef]
9. China, S.; Mazzoleni, C.; Gorkowski, K.; Aiken, A.C.; Dubey, M.K. Morphology and mixing state of individual freshly emitted wildfire carbonaceous particles. *Nat. Commun.* **2013**, *4*, 2122. [CrossRef]
10. Martins, J.V.; Artaxo, P.; Liousse, C.; Reid, J.S.; Hobbs, P.V.; Kaufman, Y.J. Effects of black carbon content, particle size, and mixing on light absorption by aerosols from biomass burning in Brazil. *J. Geophys. Res. Atmos.* **1998**, *103*, 32041–32050. [CrossRef]
11. Smith, A.J.A.; Grainger, R.G. Simplifying the calculation of light scattering properties for black carbon fractal aggregates. *Atmos. Chem. Phys.* **2014**, *14*, 7825–7836. [CrossRef]
12. Zhang, R.; Khalizov, A.F.; Pagels, J.; Zhang, D.; Xue, H.; McMurry, P.H. Variability in morphology, hygroscopicity, and optical properties of soot aerosols during atmospheric processing. *Proc. Natl. Acad. Sci. USA* **2008**, *105*, 10291–10296. [CrossRef] [PubMed]
13. Bond, T.C.; Habib, G.; Bergstrom, R.W. Limitations in the enhancement of visible light absorption due to mixing state. *J. Geophys. Res. Atmos.* **2006**, *111*, D20211. [CrossRef]
14. Cappa, C.D.; Onasch, T.B.; Massoli, P.; Worsnop, D.R.; Bates, T.S.; Cross, E.S.; Davidovits, P.; Hakala, J.; Hayden, K.L.; Jobson, B.T.; et al. Radiative Absorption Enhancements Due to the Mixing State of Atmospheric Black Carbon. *Science* **2012**, *337*, 1078–1081. [CrossRef] [PubMed]
15. Schwarz, J.P.; Gao, R.S.; Spackman, J.R.; Watts, L.A.; Thomson, D.S.; Fahey, D.W.; Ryerson, T.B.; Peischl, J.; Holloway, J.S.; Trainer, M.; et al. Measurement of the mixing state, mass, and optical size of individual black carbon particles in urban and biomass burning emissions. *Geophys. Res. Lett.* **2008**, *35*, L13810. [CrossRef]
16. Bond, T.C.; Doherty, S.J.; Fahey, D.W.; Forster, P.M.; Berntsen, T.; DeAngelo, B.J.; Flanner, M.G.; Ghan, S.; Kärcher, B.; Koch, D.; et al. Bounding the role of black carbon in the climate system: A scientific assessment. *J. Geophys. Res. Atmos.* **2013**, *118*, 5380–5552. [CrossRef]
17. Dubovik, O.; Sinyuk, A.; Lapyonok, T.; Holben, B.N.; Mishchenko, M.; Yang, P.; Eck, T.F.; Volten, H.; Muñoz, O.; Veihelmann, B.; et al. Application of spheroid models to account for aerosol particle nonsphericity in remote sensing of desert dust. *J. Geophys. Res.* **2006**, *111*, D11. [CrossRef]
18. Videen, G.; Chylek, P.J.O.C. Scattering by a composite sphere with an absorbing inclusion and effective medium approximations. *Optis Commun.* **1998**, *158*, 1–6. [CrossRef]
19. Kahnert, M.; Nousiainen, T.; Lindqvist, H. Review: Model particles in atmospheric optics. *J. Quant. Spectrosc. Radiat. Transf.* **2014**, *146*, 41–58. [CrossRef]
20. Ackerman, T.P.; Toon, O.B. Absorption of visible radiation in atmosphere containing mixtures of absorbing and nonabsorbing particles. *Appl. Opt.* **1981**, *20*, 3661–3668. [CrossRef]

21. Yin, J.Y.; Liu, L.H. Influence of complex component and particle polydispersity on radiative properties of soot aggregate in atmosphere. *J. Quant. Spectrosc. Radiat. Transf.* **2010**, *111*, 2115–2126. [CrossRef]
22. Fan, M.; Chen, L.; Li, S.; Zou, M.; Su, L.; Tao, J. The Effects of Morphology and Water Coating on the Optical Properties of Soot Aggregates. *Aerosol Air Qual. Res.* **2016**, *16*, 1315–1326. [CrossRef]
23. Dong, J.; Zhao, J.M.; Liu, L.H. Morphological effects on the radiative properties of soot aerosols in different internally mixing states with sulfate. *J. Quant. Spectrosc. Radiat. Transf.* **2015**, *165*, 43–55. [CrossRef]
24. Liu, C.; Li, J.; Yin, Y.; Zhu, B.; Feng, Q. Optical properties of black carbon aggregates with non-absorptive coating. *J. Quant. Spectrosc. Radiat. Transf.* **2017**, *187*, 443–452. [CrossRef]
25. Kahnert, M.; Nousiainen, T.; Lindqvist, H. Models for integrated and differential scattering optical properties of encapsulated light absorbing carbon aggregates. *Opt. Express* **2013**, *21*, 7974. [CrossRef] [PubMed]
26. Kahnert, M. Optical properties of black carbon aerosols encapsulated in a shell of sulfate: Comparison of the closed cell model with a coated aggregate model. *Opt. Express* **2017**, *25*, 24579–24593. [CrossRef]
27. Kahnert, M.; Kanngiesser, F. Aerosol optics model for black carbon applicable to remote sensing, chemical data assimilation, and climate modelling. *Opt. Express* **2021**, *29*, 10639–10658. [CrossRef]
28. Fuqiang, W.; Hao, W.; Dayang, G.; Ziming, C.; Lanxin, M. Radiative transfer analysis of semitransparent medium with particles having non-uniform size distribution by differential-integration method. *Int. J. Heat Mass Transf.* **2019**, *130*, 342–355. [CrossRef]
29. Ma, L.; Wang, C.; Liu, L. Polarized radiative transfer in dense dispersed media containing optically soft sticky particles. *Opt. Express* **2020**, *28*, 28252–28268. [CrossRef]
30. Aoyu, Z.; Fuqiang, W.; Ziming, C.; Huaxu, L.; Xuhang, S. Radiative property investigation of dispersed particulate medium with the consideration of non-uniform particle size distribution and dependent scattering effects. *Int. J. Heat Mass Transf.* **2022**, *186*, 122488. [CrossRef]
31. Liu, C. Optical Properties of Black Carbon Aggregates. In *Springer Series in Light Scattering. Volume 3: Radiative Transfer and Light Scattering*; Springer Series in Light Scattering; Springer: Berlin/Heidelberg, Germany, 2019; pp. 167–218.
32. Bao, Y.; Huang, Y.; Li, W.; Zhu, K. Comparison of the scattering properties between TiO2 and ITO clusters based on the particle superposition model. *Opt. Mater. Express* **2019**, *9*, 562–575. [CrossRef]
33. Witten, T.A.; Sander, L.M. Diffusion-Limited Aggregation in Three Dimensions. *Phys. Rev. B Condens. Matter* **1983**, *27*, 5686–5697. [CrossRef]
34. Prasanna, S.; Rivière, P.; Soufiani, A. Effect of fractal parameters on absorption properties of soot in the infrared region. *J. Quant. Spectrosc. Radiat. Transf.* **2014**, *148*, 141–155. [CrossRef]
35. Wu, Y.; Cheng, T.; Zheng, L.; Chen, H. Effect of morphology on the optical properties of soot aggregated with spheroidal monomers. *J. Quant. Spectrosc. Radiat. Transf.* **2016**, *168*, 158–169. [CrossRef]
36. Tianhai Cheng, X.G.; Yu, W.; Hao, C. Effects of atmospheric water on the optical properties of soot aerosols with different mixing states. *J. Quant. Spectrosc. Radiat. Transf.* **2014**, *147*, 196–206. [CrossRef]
37. Yu, H.-T.; Liu, D.; Duan, Y.-Y.; Wang, X.-D. Theoretical model of radiative transfer in opacified aerogel based on realistic microstructures. *Int. J. Heat Mass Transf.* **2014**, *70*, 478–485. [CrossRef]
38. Christopher, M.; Sorensen, G.C.R. The Prefactor of Fractal Aggregates. *J. Colloid Interface Sci.* **1997**, *186*, 447–452. [CrossRef]
39. Forrest, S.R.; Witten, T.A. Long-range correlations in smoke-particle aggregates. *J. Phys. A Math. Gen.* **1979**, *12*, L109–L117. [CrossRef]
40. Sorensen, C.M. Light Scattering by Fractal Aggregates: A Review. *Aerosol Sci. Technol.* **2001**, *35*, 648–687. [CrossRef]
41. Bond, T.C.; Bergstrom, R.W. Light Absorption by Carbonaceous Particles: An Investigative Review. *Aerosol Sci. Technol.* **2006**, *40*, 27–67. [CrossRef]
42. Luo, J.; Zhang, Y.; Wang, F.; Zhang, Q. Effects of brown coatings on the absorption enhancement of black carbon: A numerical investigation. *Atmos. Chem. Phys.* **2018**, *18*, 16897–16914. [CrossRef]
43. Kahnert, M.; Nousiainen, T.; Lindqvist, H.; Ebert, M. Optical properties of light absorbing carbon aggregates mixed with sulfate: Assessment of different model geometries for climate forcing calculations. *Opt. Express* **2012**, *20*, 10042–10058. [CrossRef] [PubMed]
44. Huang, Y.; Zhao, R.; Li, W. Radiative characteristics of nonspherical particles based on a particle superposition model. *J. Geophys. Res. Atmos.* **2013**, *118*, 11–762. [CrossRef]
45. Huang, Y.; Jin, C.; Bao, Y. Effects of bump/pit on the radiative properties of small particles. *Opt. Lett.* **2016**, *41*, 1455–1457. [CrossRef] [PubMed]
46. Tang, Y.; Zhu, K.; Huang, Y. Radiative properties of porous fly ash particles based on the particle superposition model. *J. Quant. Spectrosc. Radiat. Transf.* **2022**, *277*, 107977. [CrossRef]
47. Purcell, E.M.; Pennypacker, C.R. Scattering and Absorption of Light by Nonspherical Dielectric Grains. *Astrophys. J.* **1973**, *186*, 705–714. [CrossRef]
48. Draine, B.T. The Discrete-Dipole Approximation and Its Application to Interstellar Graphite Grains. *Astrophys. J.* **1988**, *333*, 848–872. [CrossRef]
49. Draine, B.T.; Flatau, P.J. Discrete-Dipole Approximation for Scattering Calculations. *J. Opt. Soc. Am. A* **1994**, *11*, 1491–1499. [CrossRef]
50. Draine, B.T.; Flatau, P.J. User guide for the discrete dipole approximation code DDSCAT 7.3. *arXiv* **2013**, arXiv:1305.6497.

51. Draine, B.T.; Flatau, P.J. Discrete-dipole approximation for periodic targets: Theory and tests. *J. Opt. Soc. Am. A* **2008**, *25*, 1491–1499. [CrossRef]
52. Flatau, P.; Draine, B. Fast near field calculations in the discrete dipole approximation for regular rectilinear grids. *Opt. Express* **2012**, *20*, 1247–1252. [CrossRef]
53. Flatau, P.; Draine, B. Light scattering by hexagonal columns in the discrete dipole approximation. *Opt. Express* **2014**, *22*, 21834–21846. [CrossRef] [PubMed]
54. Draine, B.; Goodman, J. Beyond Clausius-Mossotti—Wave propagation on a polarizable point lattice and the discrete dipole approximation. *Astrophys. J.* **1993**, *405*, 685–697. [CrossRef]
55. Travis, L.; Lacis, A. *Scattering, Absorption, and Emission of Light by Small Particles*; Cambridge University Press: New York, NY, USA, 2002; Volume 4.
56. Kandilian, R.; Heng, R.-L.; Pilon, L. Absorption and scattering by fractal aggregates and by their equivalent coated spheres. *J. Quant. Spectrosc. Radiat. Transf.* **2015**, *151*, 310–326. [CrossRef]
57. Mishchenko, M.I. Light scattering by randomly oriented axially symmetric particles. *J. Opt. Soc. Am. A* **1991**, *8*, 871–882. [CrossRef]
58. Nousiainen, T.; Kahnert, M.; Lindqvist, H. Can particle shape information be retrieved from light-scattering observations using spheroidal model particles? *J. Quant. Spectrosc. Radiat. Transf.* **2011**, *112*, 2213–2225. [CrossRef]
59. Li, J.; Liu, C.; Yin, Y.; Kumar, K.R. Numerical investigation on the Ångström exponent of black carbon aerosol. *J. Geophys. Res. Atmos.* **2016**, *121*, 3506–3518. [CrossRef]